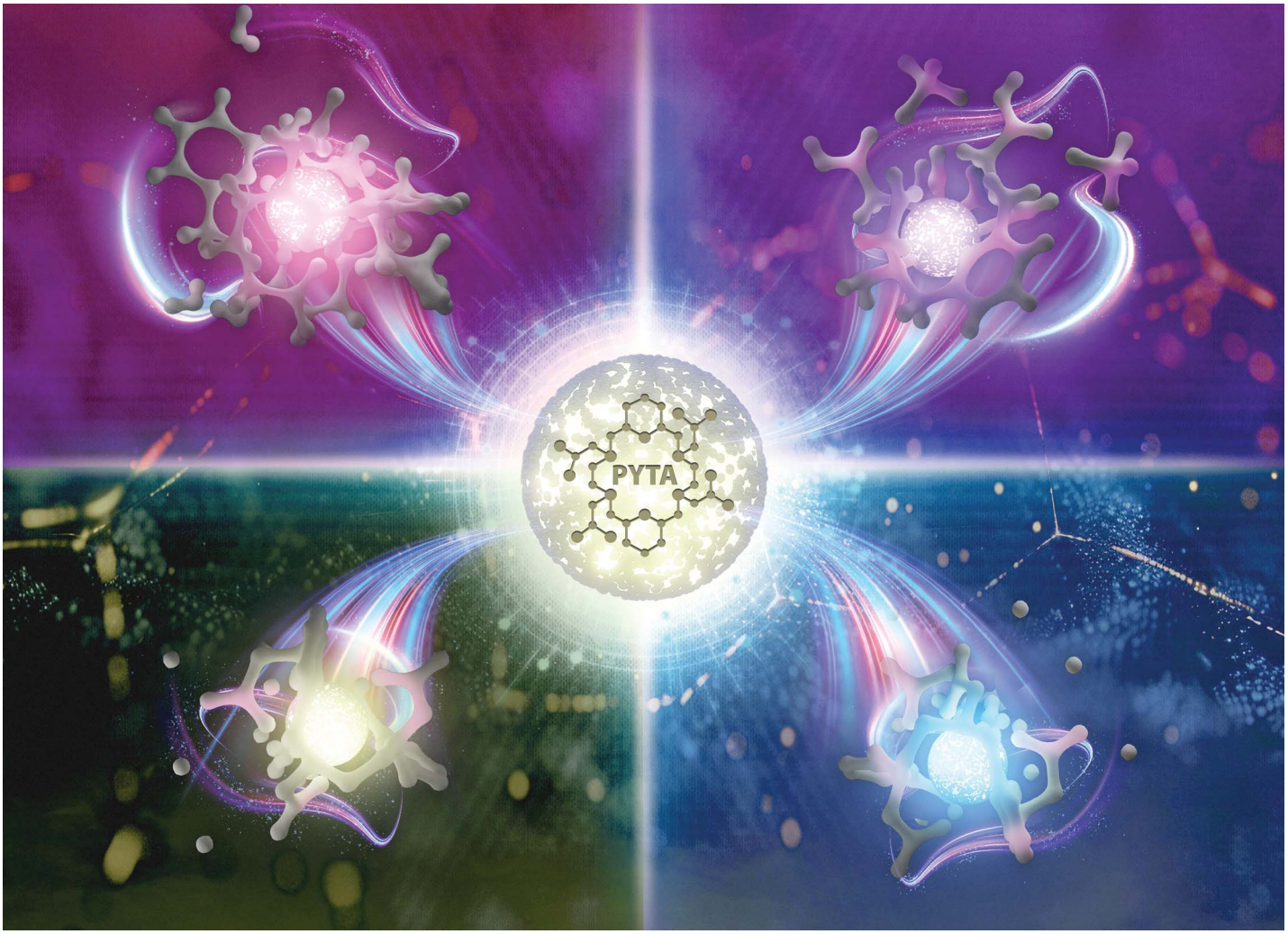

Showcasing research from the laboratories of Drs. Nikki Thiele and Frankie White at Oak Ridge National Laboratory, USA and Prof. Daniel Thorek at Washington University in St. Louis, USA.

PYTA: a universal chelator for advancing the theranostic palette of nuclear medicine

This work reports the chelation properties of PYTA with ^{225}Ac, ^{177}Lu, ^{111}In, and ^{44}Sc, a "superfecta" of complementary but chemically distinct radiometals for targeted alpha and beta therapy, single-photon emission computed tomography, and positron-emission tomography, respectively. In vitro and in vivo studies reveal PYTA to rapidly bind and stabilize these radiometals, establishing proof-of-principle for the use of PYTA in targeted theranostic radiopharmaceuticals. Image courtesy of Adam Malin, Oak Ridge National Laboratory.

As featured in:

See Frankie D. White, Daniel L. J. Thorek, Nikki A. Thiele *et al.*, *Chem. Sci.*, 2024, **15**, 11279.

ROYAL SOCIETY OF CHEMISTRY

rsc.li/chemical-science

Registered charity number: 207890

Chemical Science

ROYAL SOCIETY OF CHEMISTRY

EDGE ARTICLE

View Article Online
View Journal | View Issue

Cite this: *Chem. Sci.*, 2024, **15**, 11279

All publication charges for this article have been paid for by the Royal Society of Chemistry

PYTA: a universal chelator for advancing the theranostic palette of nuclear medicine†

Megan E. Simms, ‡§[a] Zhiyao Li,‡[bc] Megan M. Sibley, [a] Alexander S. Ivanov, [a] Caroline M. Lara, [d] Timothy C. Johnstone, [e] Vilmos Kertesz, [f] Amanda Fears,[bc] Frankie D. White, *[g] Daniel L. J. Thorek *[bchi] and Nikki A. Thiele *[a]

To clinically advance the growing arsenal of radiometals available to image and treat cancer, chelators with versatile binding properties are needed. Herein, we evaluated the ability of the py_2[18]dieneN$_6$ macrocycle PYTA to interchangeably bind and stabilize $^{225}Ac^{3+}$, [^{177}Lu]Lu^{3+}, [^{111}In]In^{3+} and [^{44}Sc]Sc^{3+}, a chemically diverse set of radionuclides that can be used complementarily for targeted alpha therapy, beta therapy, single-photon emission computed tomography (SPECT) imaging, and positron emission tomography (PET) imaging, respectively. Through NMR spectroscopy and X-ray diffraction, we show that PYTA possesses an unusual degree of flexibility for a macrocyclic chelator, undergoing dramatic conformational changes that enable it to optimally satisfy the disparate coordination properties of each metal ion. Subsequent radiolabeling studies revealed that PYTA quantitatively binds all 4 radiometals at room temperature in just minutes at pH 6. Furthermore, these complexes were found to be stable in human serum over 2 half-lives. These results surpass those obtained for 2 state-of-the-art chelators for nuclear medicine, DOTA and macropa. The stability of ^{225}Ac–PYTA and [^{44}Sc]Sc–PYTA, the complexes having the most disparity with respect to metal-ion size, was further probed in mice. The resulting PET images (^{44}Sc) and *ex vivo* biodistribution profiles (^{44}Sc and ^{225}Ac) of the PYTA complexes differed dramatically from those of unchelated [^{44}Sc]Sc^{3+} and $^{225}Ac^{3+}$. These differences provide evidence that PYTA retains this size-divergent pair of radionuclides *in vivo*. Collectively, these studies establish PYTA as a new workhorse chelator for nuclear medicine and warrant its further investigation in targeted constructs.

Received 20th December 2023
Accepted 5th June 2024

DOI: 10.1039/d3sc06854d

rsc.li/chemical-science

Introduction

Radioactive isotopes of metal ions across the periodic table, from alkalis to actinides, are increasingly being explored in the clinic to diagnose and treat cancer.[1–4] The use of radiometals in this context leverages the unique ionizing emissions afforded by nuclear decay. Radiometals that emit positrons (β^+) or gamma (γ) rays can be used to image lesions *via* positron emission tomography (PET) or single-photon emission computed tomography (SPECT), respectively.[5] By contrast, therapy can be achieved using radiometals that emit cytotoxic alpha (α) particles, beta (β^-) particles, or Meitner–Auger electrons.[6,7] When paired together, diagnostic and therapeutic radiometals with complementary properties can form powerful "theranostic" platforms to provide precise information about disease localization, dosimetry, and treatment response.[8] Consequently, this information can be harnessed to develop treatment plans tailored to the individual patient.[9]

Irrespective of emission type, a universal requirement for the implementation of radioactive metal ions in targeted nuclear medicine is their attachment to tumor-seeking carrier

[a]*Chemical Sciences Division, Oak Ridge National Laboratory, Oak Ridge, TN 37831, USA. E-mail: thielena@ornl.gov*

[b]*Department of Radiology, Washington University in St. Louis School of Medicine, St. Louis, MO 63110, USA. E-mail: thorekd@wustl.edu*

[c]*Program in Quantitative Molecular Therapeutics, Washington University in St. Louis School of Medicine, St. Louis, MO 63110, USA*

[d]*Department of Biological Sciences, University of Notre Dame, Notre Dame, IN 46556, USA*

[e]*Department of Chemistry and Biochemistry, University of California Santa Cruz, Santa Cruz, CA 95064, USA*

[f]*Biosciences Division, Oak Ridge National Laboratory, Oak Ridge, TN 37831, USA*

[g]*Radioisotope Science and Technology Division, Oak Ridge National Laboratory, Oak Ridge, TN 37831, USA. E-mail: whitefd@ornl.gov*

[h]*Department of Biomedical Engineering, Washington University in St. Louis, St. Louis, MO 63110, USA*

[i]*Oncologic Imaging Program, Siteman Cancer Center, Washington University in St. Louis School of Medicine, St. Louis, MO 63110, USA*

† Electronic supplementary information (ESI) available: Experimental procedures, NMR and X-ray characterization data, DFT calculations, animal protocols, and representative radio-TLC chromatograms. CCDC 2297429, 2297430, and 2339314. For ESI and crystallographic data in CIF or other electronic format see DOI: **https://doi.org/10.1039/d3sc06854d**

‡ These authors contributed equally to this work.

§ Present address: Radioisotope Science and Technology Division, Oak Ridge National Laboratory, Oak Ridge, TN 37831, United States.

molecules, such as antibodies or peptides, *via* bifunctional chelators. This attachment ensures that each radiometal is selectively delivered to sites of disease, minimizing off-target radiotoxicity to healthy organs. In this regard, the formation of metal–chelator complexes of high thermodynamic and kinetic stability is crucial to prevent dissociation *in vivo*. To achieve this stability, many ligand design efforts have focused on matching and optimizing the structure of a chelator to the coordination preferences of a single radiometal ion of interest.[10] This strategy has enabled significant advances over the last decade in the development of new metal-based radiopharmaceuticals.[11–13] However, as the number and chemical diversity of medically useful radiometals continues to expand, ligand development using the conventional one-metal–one-chelator paradigm has struggled to keep pace. With a shortage of suitable chelators for the ever-growing nuclear chocolate box,[1] the advancement of many emerging radiometals has been halted in the so-called "valley of death" between production and clinical implementation, unable to reach their full medicinal potential.

To address this challenge, new efforts have been directed towards developing chelators for nuclear medicine that exhibit more versatile binding properties. For example, the 18-membered macrocycles macrodipa,[14] py-macrodipa[15] and py_2-macrodipa[16] (see Fig. S1 in the ESI†) were developed recently as dual-size-selective chelators for binding both large and small radioactive rare-earth ions, such as the Meitner–Auger-electron emitter lanthanum-135 ($^{135}La^{3+}$, 8-coordinate ionic radius = 1.16 Å)[17] and the β^+ emitter scandium-44 ($^{44}Sc^{3+}$, 8-coordinate ionic radius = 0.87 Å),[17] respectively. Several high denticity acyclic bispidine[18,19] and picolinic acid[20,21] chelators have also been identified to mutually stabilize the α-emitting radionuclide actinium-225 (^{225}Ac) and either indium-111 (^{111}In), a SPECT radionuclide, or lutetium-177 (^{177}Lu), a therapeutic β^- emitter with imageable γ emissions (Fig. S1†). With respect to metal-binding range, however, the 12-membered tetraaza macrocycle DOTA (Scheme 1) remains unsurpassed in its ability to stabilize a wide assortment of radiometals with disparate chemical and physical properties. DOTA plays a central role in theranostics as the bifunctional chelator in several clinically approved gallium-68 (^{68}Ga) and ^{177}Lu radiopharmaceuticals for PET imaging and targeted β^- therapy of cancer, respectively.[22–25] Targeted constructs comprising DOTA are also being investigated in clinical trials for use with copper-64 (^{64}Cu) for PET[26,27] and with ^{225}Ac and other α emitters for targeted α therapy (TAT).[28,29]

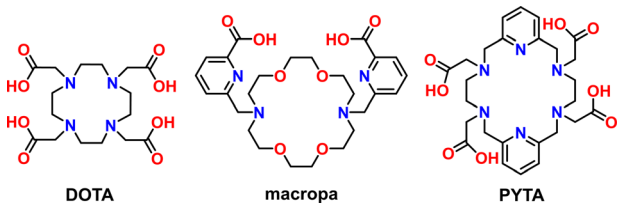

Scheme 1 Chemical structures of the chelators used in this work.

Despite its demonstrated versatility, one prominent shortcoming of DOTA is its inability to chelate most radiometals at room temperature. Although its slow complex formation kinetics can be overcome by heating these radiolabeling reactions, high temperatures are not compatible with the use of thermolabile biological targeting vectors, such as antibodies. As such, the development of alternative chelators that retain DOTA's broad chelation properties but radiolabel rapidly at low temperature would be highly valuable for use in nuclear medicine. Notably, there is a strong preference for peptide or antibody conjugates to use a single chelator for both imaging and therapy because it would have nearly identical pharmacokinetic properties and simplify regulatory filing, as only a single chemical entity would need to be advanced to production, quality control, and clinical evaluation.

Towards this end, we sought to investigate the radiometal chelation properties of a macrocyclic ligand called PYTA (Scheme 1). Like DOTA, PYTA possesses four tetraacetic acid pendent arms, but has a core 18-membered macrocycle into which two pyridine rings are embedded. Previous studies have demonstrated that PYTA and related pendent-arm derivatives form remarkably stable complexes with a variety of non-radioactive transition and rare-earth metal ions and may be useful as magnetic resonance imaging (MRI) contrast agents.[30–38] While our studies were underway, a triacetic acid derivative of PYTA for the chelation of radio-yttrium was reported.[39] However, the suitability of PYTA itself as a chelator for targeted radiopharmaceutical applications has remained largely unexplored.[30] In this work, we evaluated the ability of PYTA to complex $^{225}Ac^{3+}$, $^{177}Lu^{3+}$, $^{111}In^{3+}$, and $^{44}Sc^{3+}$, a complementary suite of theranostic α-, β^--, γ-, and β^+-emitting radiometal ions, respectively. These radiometals were selected because they are among the most intensely investigated for use in targeted radiopharmaceutical development and translation, yet have been extremely challenging to bind using a single chelator due to their significant differences in ionic radii (Table 1) and coordination chemistries. Through a combination of structural, radiolabeling, serum stability, and *in vivo* studies,

Table 1 Comparison of average interatomic distances (Å) and angles (°) observed in the X-ray crystal structures of La^{3+}, Lu^{3+}, In^{3+}, and Sc^{3+} complexes of PYTA[a]

	La[b]	Lu[b]	In[c]	Sc[c]
Ionic radius[d]	1.160	0.977	0.92	0.870
Space group	$P2_1/n$	$C2/c$	$R\bar{3}c$	$C2/c$
$M–N_{py}$	2.637(1)	2.508(2)	2.3401(10)	2.463(4)
$M–N_{amine}$	2.702(10)	2.594(27)	2.523(89)	2.578(49)
$M–O_{carb}$[e]	2.604(69)	2.250(5)	2.1328(10)	2.137(5)
$N_{py}–M–N_{py}$	178.40(7)	146.45(7)	108.58(5)	146.04(5)

[a] Values in parentheses are one standard deviation (of the last significant figures) from the average of crystallographically independent values. In instances where there is only one crystallographically independent value, the standard uncertainty of the refined value is reported. [b] From ref. 32. [c] This work. [d] Eight-coordinate ionic radii from ref. 17. [e] Averages were taken according to the number of carboxylic acid functional groups bound to the metal center (La, 4; Lu and Sc, 3; In, 2).

we demonstrate that PYTA can rapidly chelate all four radiometals at room temperature, forming complexes that are highly stable under physiological conditions. These results establish PYTA as one of the most versatile chelators investigated to date for theranostic applications.

Results and discussion

PYTA was synthesized according to published procedures,[32,40] with minor modifications (see Section 1 of the ESI†). As a first assessment of the suitability of PYTA for the chelation of ^{225}Ac, ^{177}Lu, ^{111}In, and ^{44}Sc, its solution-state chemistry with La^{3+}, Lu^{3+}, In^{3+}, and Sc^{3+} was probed by ^{1}H nuclear magnetic resonance (NMR) spectroscopy in D_2O. Ac^{3+} was substituted with La^{3+} for this study because Ac^{3+} does not possess any stable isotopes, rendering the obtention of NMR spectra challenging.[41] La^{3+} is often used as a surrogate for Ac^{3+} because of its similar chemical properties and only slightly smaller ionic radius (1.160 Å for 8-coordinate La^{3+}, 1.220 Å for 9-coordinate Ac^{3+}).[17,42] Our density functional theory calculations and *ab initio* molecular dynamics simulations reveal similarities between La^{3+} and Ac^{3+} coordination by PYTA, supporting the notion that the La^{3+} complex approximates the Ac^{3+} complex in solution (Section S2, Fig. S2 and Table S1†). NMR samples were prepared at pH ∼ 7 using equimolar amounts of chelator and metal ion, and their spectra were acquired after 1 h at room temperature, except for the La^{3+}–PYTA sample, which required further heating at 60 °C (unoptimized) to drive the complexation reaction to completion (Section S3†). High-resolution mass spectrometry confirmed complex formation for all samples (Fig. S3–S6†).

The NMR spectra obtained for La^{3+} and Lu^{3+} (Fig. S7†) were similar to those reported previously.[32] Specifically, complexation of La^{3+} by PYTA gave rise to 8 sharp signals, indicating the formation of a D_2-symmetric complex in which all pendent arms are bound to the metal center in a rigid 10-coordinate configuration. By contrast, the Lu^{3+} spectrum was consistent with an asymmetric 9-coordinate complex. This configuration was evident from the presence of 2 triplets and 2 doublets for the 6 pyridyl protons of the chelator, which signals that the pyridyl groups experience different magnetic environments. Additionally, a singlet was observed at 4.22 ppm, which can be assigned to the methylene protons of one uncoordinated acetate arm.

The spectrum of the Sc–PYTA complex (Fig. S7†) matched closely to that of the Lu–PYTA complex, indicating a shared 9-coordinate structural conformation. By contrast, the spectrum of the In–PYTA complex was less straightforward to interpret (Fig. S7†). Broadening of the aliphatic resonances precluded any meaningful analysis of this region. However, two sets of signals can be discerned in the aromatic region in approximately a 65/35 ratio, one set belonging to a symmetric species (major) and the other to an asymmetric species (minor). Upon heating the sample to 90 °C, the two sets of aromatic signals were observed to coalesce (Fig. S8†). These findings are consistent with the existence of two configurational isomers in solution undergoing slow exchange on the NMR timescale. Another notable feature of the In–PYTA spectrum is that the aromatic resonances are shifted considerably downfield in comparison to those of the other complexes. This shift may signify that the pyridyl groups of PYTA are positioned closer to the electron-withdrawing metal center when chelating In^{3+} *versus* La^{3+}, Lu^{3+}, and Sc^{3+}. Collectively, the differences observed in the spectra of these complexes in aqueous solution point

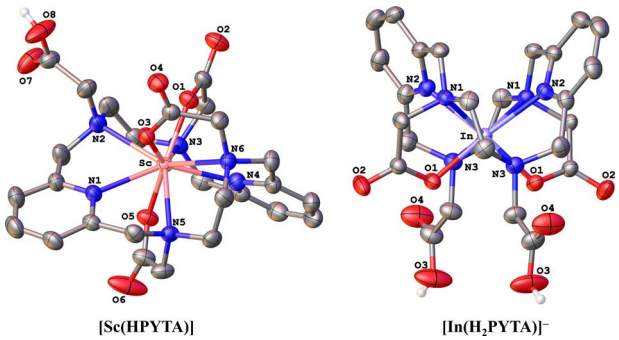

Fig. 1 X-ray crystal structures of Sc^{3+} (left) and In^{3+} (right) complexes of PYTA. Ellipsoids for carbons and heteroatoms are drawn at the 50% probability level. Counteranions, outer-sphere solvent molecules, and hydrogen atoms attached to carbon centers have been omitted for the sake of clarity.

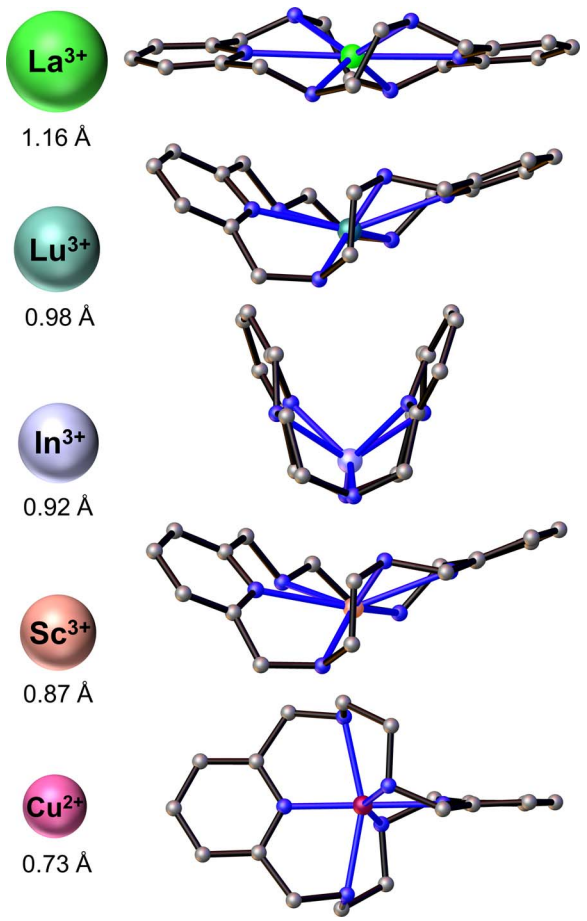

Fig. 2 Configuration of the macrocyclic backbone of PYTA when bound to La^{3+}, Lu^{3+}, In^{3+}, Sc^{3+}, or Cu^{2+}. 8-Coordinate ionic radii (6-coordinate for Cu^{2+}) are provided below each metal ion. Pendent acetate arms have been omitted for clarity.

towards the flexibility of PYTA to adopt the configurations necessary to satisfy the coordination preferences of a range of metal ions.

To further interrogate the structural changes that PYTA undergoes upon binding these metals, we obtained single-crystal structures of its Sc^{3+} and In^{3+} complexes (Fig. 1) and compared them to the published crystal structures of its La^{3+} and Lu^{3+} complexes, $[La(H_2PYTA)](NO_3)\cdot 3H_2O$ and $[Lu(HPYTA)]\cdot 3H_2O$.[32] Select interatomic distances and angles are presented in Table 1, and additional details of the crystallographic refinement are provided in Section S4 and Table S2.† The Sc^{3+} complex crystallized in the $C2/c$ space group as $[Sc(HPYTA)]\cdot 3H_2O$ (Fig. 1), with a conformation that is isostructural to that of the Lu^{3+} complex. Specifically, 3 of the 4 pendent arms are deprotonated and engaged in binding interactions with the metal center, giving rise to a 9-coordinate complex that is consistent with our NMR analysis. Additionally, the pyridine rings of the core macrocycle are twisted away from one another and folded inward towards the metal center (Fig. 2), giving rise to a N_{py}–M–N_{py} angle of 146.04(5)° (Table 1). This "twist-fold" conformation is typical for PYTA when complexing smaller lanthanide ions, whereas the macrocycle adopts a more planar structure when binding larger ions like La^{3+} (Fig. 2, N_{py}–M–N_{py} = 178.40(7)°).[32]

Interestingly, In–PYTA crystallized in the $R\bar{3}c$ space group as the 8-coordinate C_2-symmetric complex $[In(H_2PYTA)]ClO_4$ (Fig. 1). This result was somewhat unexpected because the ionic radius of In^{3+} is intermediate between that of Lu^{3+} and Sc^{3+} (Table 1). If the conformation of PYTA were driven exclusively by the size of the metal ion, the In–PYTA complex would be expected to crystallize in a configuration similar to that of Lu–PYTA and Sc–PYTA. Instead, for the In^{3+} structure, two acetate groups of PYTA remain protonated and uncoordinated, and the macrocyclic backbone is folded nearly in half (Fig. 2; N_{py}–M–N_{py} = 108.58(5)°). This complex represents an extreme example of the twist-fold conformation[32] that has not been observed previously for py_2[18]dieneN_6 macrocycles, to the best of our knowledge. As the NMR data suggested, this conformation allows for the macrocycle to be drawn closer to the metal center, leading to shorter average interatomic metal-donor distances than expected based on the ionic radius of In^{3+} (Table 1). This divergent configuration in comparison to the other complexes likely arises from differences in the aqueous chemistry of In^{3+} *versus* La^{3+}, Lu^{3+}, and Sc^{3+}. Although all 4 ions are classified as relatively "hard" according to Pearson's hard-soft acid–base theory,[43–45] the ionicity (I_A) of In^{3+}, taken as the ratio of the electrostatic and covalent contributions to bonding, is lower than that of La^{3+}, Lu^{3+}, and Sc^{3+} (6.30 *versus* 10.30, 10.07, and 10.49, respectively).[46–49] Moreover, In^{3+} typically forms complexes with lower coordination numbers ranging from 4 to 8.[50,51] These properties may be expected to direct the configuration of the In–PYTA complex to one that cannot be predicted on the basis of ion size. As a final demonstration of the extreme versatility of PYTA, its crystal structure was obtained with Cu^{2+}, a chemically softer, divalent metal ion with a 6-coordinate ionic radius of only 0.73 Å[17] and an I_A of 2.68.[43–45] In this structure (Fig. S9 and Table S2†), all pendent arms remain unbound, and the nitrogen atoms of the macrocycle are arranged in a pseudo-octahedral geometry around

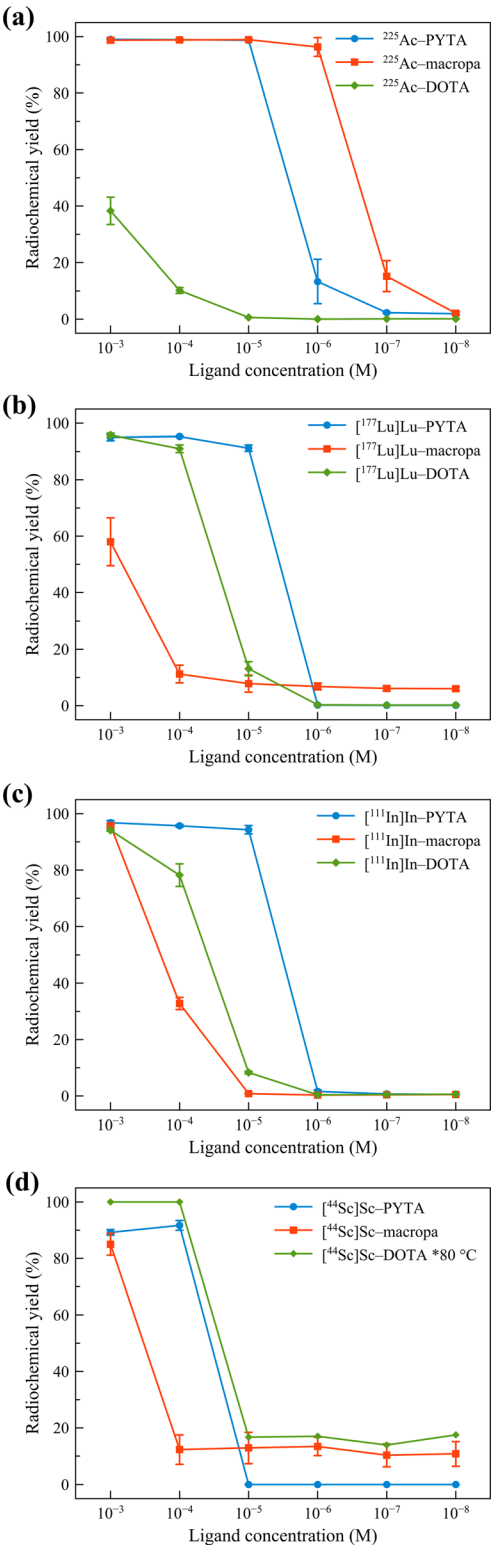

Fig. 3 Concentration-dependent radiolabeling of PYTA, macropa, and DOTA with (a) $^{225}Ac^{3+}$ (9.3–11.1 kBq), (b) $[^{177}Lu]Lu^{3+}$ (22–37 kBq), (c) $[^{111}In]In^{3+}$ (74–111 kBq), and (d) $[^{44}Sc]Sc^{3+}$ (185 kBq) after 5 min reaction time. All reactions were carried out at room temperature in NH_4OAc (0.5 M, pH 6.0) except for $[^{44}Sc]$Sc–DOTA, which was at 80 °C, V_T = 150 μL. The error bars represent the standard deviations. Data for ^{225}Ac–macropa and ^{225}Ac–DOTA were taken from ref. 16.

the Cu center. This "twist-wrap" conformation of PYTA,[32] shown in Fig. 2, is likewise adopted by the unfunctionalized py_2[18]dieneN_6 macrocycle when bound to Cu^{2+}.[52]

With these results in hand demonstrating that PYTA can accommodate a range of disparate metal ions by dramatically changing its conformation, we next sought to evaluate PYTA's ability to bind and stabilize ^{225}Ac ($t_{1/2} = 10.0$ d), ^{177}Lu ($t_{1/2} = 6.65$ d), ^{111}In ($t_{1/2} = 2.80$ d), and ^{44}Sc ($t_{1/2} = 3.97$ h). Concentration-dependent radiolabeling experiments were performed in pH 6 NH_4OAc buffer at room temperature (RT). Radiochemical yields (RCYs) were assessed after 5 min and 60 min using radio-thin layer chromatography (Table S3 and Fig. S10–S23†). To benchmark the performance of PYTA, we also conducted additional radiolabeling experiments with DOTA and macropa (Table S3 and Fig. S10–S23†). Macropa (Scheme 1) was included for comparison because of its rare ability to rapidly form stable complexes with ^{225}Ac and other large radiometals at room temperature.[53–56] The results of the radiolabeling studies are collected in Fig. 3 and S24.†

Remarkably, quantitative radiolabeling of PYTA was achieved with ^{225}Ac, ^{177}Lu, and ^{111}In in just 5 min at chelator concentrations as low as 1×10^{-5} M. Likewise, PYTA was able to complex nearly all the ^{44}Sc at a chelator concentration of 1×10^{-4} M (and down to 4×10^{-5} M, measured at 60 min only). We note that for all studies, a second, minor peak was observed in the radio-TLCs of ^{44}Sc control samples regardless of the type of plate or mobile phase used. This small portion of activity, which remained unchelated even at the highest PYTA concentrations, has been attributed previously to the formation of insoluble (or difficult-to-chelate) oxide/hydroxide species.[57] Increasing the mixing time to 60 min for ^{225}Ac, ^{177}Lu, ^{111}In, and ^{44}Sc reactions did not give rise to higher RCYs, indicating that complexation equilibrium was reached rapidly for each radionuclide. Under the same conditions, DOTA was found to be a less effective chelator than PYTA for ^{225}Ac, ^{177}Lu, and ^{111}In, even after allowing the reactions to proceed for 60 min (Fig. S24†) and heating them to 80 °C (Fig. S25†). This inferior labeling efficacy is reflected by the low RCYs of 1%, 44%, and 24% obtained for ^{225}Ac, ^{177}Lu, and ^{111}In at 10^{-5} M chelator concentration, 60 min, and RT, conditions under which PYTA is quantitatively radiolabeled. Radiolabeling of DOTA with ^{44}Sc at 80 °C gave rise to RCYs on par with those obtained for PYTA (Fig. 3 and S24†) but was observed to be inconsistent at room temperature (Fig. S22†). Similarly, the RCYs of macropa were also substantially lower than those of PYTA for ^{177}Lu, ^{111}In, and ^{44}Sc, but higher for ^{225}Ac (Fig. 3 and S24†). These results are in line with macropa's exceptional ability to bind large metal ions like Ac^{3+} but correspondingly low affinity for smaller metal ions like Lu^{3+}, In^{3+} and Sc^{3+}.

Following these radiolabeling studies, the kinetic inertness of the resulting complexes of PYTA, DOTA, and macropa with ^{225}Ac, ^{177}Lu, ^{111}In, and ^{44}Sc (PYTA only) were investigated in 75% human serum at 37 °C. Human serum contains a variety of endogenous ligands and proteins that may compete with a chelator for metal binding, and therefore serves as a challenge to indicate the likelihood of transchelation *in vivo*. TLC systems and chelator concentrations used in these challenges, as well as representative radio-TLC traces, are provided in Table S4 and Fig. S26–S37.† The percentages of intact complexes over time are compiled in Table 2. Impressively, ^{225}Ac–PYTA, [^{177}Lu]Lu–PYTA, [^{111}In]In–PYTA, and [^{44}Sc]Sc–PYTA all remained ≥95% intact in serum over the course of two half-lives of the respective radionuclides. Similar results were also observed for DOTA, which retained 88%, 97%, and 96% of $^{225}Ac^{3+}$, [^{177}Lu]Lu^{3+} and [^{111}In]In^{3+} over the course of the study. It should be noted, however, that due to DOTA's subpar radiolabeling efficacy, the concentration of DOTA required in the ^{177}Lu and ^{111}In studies (10^{-4} M) to ensure complex formation at the start of the experiment was an order of magnitude higher than the concentration used for PYTA (10^{-5} M). Like PYTA and DOTA, macropa also formed a highly stable complex with ^{225}Ac, releasing <3% of bound ^{225}Ac over 21 d. By contrast, [^{177}Lu]Lu–macropa completely dissociated within the first hour of the experiment, and [^{111}In]In–macropa underwent 75% decomplexation within 1 d. Interestingly, when a higher concentration of macropa (8.4×10^{-4} M *vs.* 1×10^{-4} M) was used in the ^{111}In

Table 2 Stability (% intact complex remaining) measured at various time points after incubating the $^{225}Ac^{3+}$, [^{177}Lu]Lu^{3+}, [^{111}In]In^{3+}, and [^{44}Sc]Sc^{3+} complexes of PYTA, macropa, and DOTA in 75% human serum at 37 °C[a,b]

Complex	Before serum addition	1 h	2 h	8 h	1 d	2 d	3 d	4 d	7 d	14 d	21 d
^{225}Ac–PYTA[d]	100	99	ND	ND	98	99	99	98	97	95	**95**
^{225}Ac–macropa[c,d]	100	99	ND	ND	99	99	99	ND	99	98	**97**
^{225}Ac–DOTA[d]	99	98	ND	ND	98	97	96	ND	94	89	**88**
[^{177}Lu]Lu–PYTA[d]	100	99	ND	ND	99	99	98	98	99	**98**	ND
[^{177}Lu]Lu–macropa[e]	82	0.6	ND	ND	**0.9**	ND	ND	ND	ND	ND	ND
[^{177}Lu]Lu–DOTA[f]	99	98	ND	ND	99	99	98	ND	98	**97**	ND
[^{111}In]In–PYTA[d]	97	97	ND	ND	97	95	96	**97**	ND	ND	ND
[^{111}In]In–macropa[g]	99	95	ND	ND	87	91	93	**92**	ND	ND	ND
[^{111}In]In–macropa[f]	99	95	ND	ND	**25**	ND	ND	ND	ND	ND	ND
[^{111}In]In–DOTA[f]	98	98	ND	ND	96	96	95	**96**	ND	ND	ND
[^{44}Sc]Sc–PYTA[d]	94	94[h]	95	93	ND	ND	ND	ND	ND	ND	ND

[a] Standard deviations for all values are ≤2%. Bolded values indicate stability at the final time point. [b] ND = not determined. [c] Data taken from ref. 16. [d] $C_{chelator} = 1 \times 10^{-5}$ M. [e] $C_{chelator} = 1 \times 10^{-3}$ M. [f] $C_{chelator} = 1 \times 10^{-4}$ M. [g] $C_{chelator} = 8.4 \times 10^{-4}$ M. [h] Measured at $t = 30$ min.

serum challenge, a dramatic rise in complex stability to 92% at 4 d was noted. This increase in intact complex with increasing chelator concentration is likely a thermodynamic effect arising from metal–ligand recombination in solution in the closed-tube system used for these studies, rather than a reflection of enhanced kinetic stability. Collectively, the radiolabeling studies and serum challenges reveal PYTA to be far superior to DOTA and macropa for rapidly binding and stabilizing this "superfecta" of medical radionuclides under mild, physiologically relevant conditions.

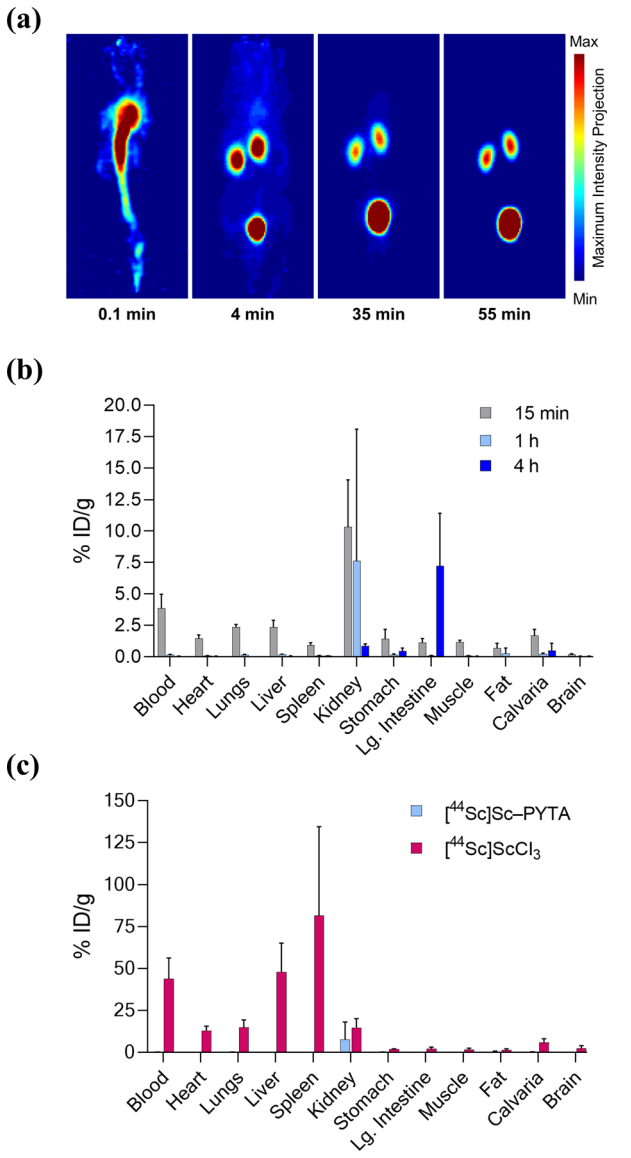

Fig. 4 PET imaging and *ex vivo* biodistribution of [^{44}Sc]Sc–PYTA in female Swiss Webster mice (6–8 weeks, $n = 4$ per time point) following intravenous injection. (a) Representative 3D maximum intensity projections of the PET acquisitions at 0.1, 4, 35, and 55 min post injection indicating rapid transit from the blood pool to the kidneys and bladder. (b) Biodistribution of [^{44}Sc]Sc–PYTA for select organs after 15 min, 1 h, and 4 h post injection. (c) Comparison of biodistribution of [^{44}Sc]Sc–PYTA and [^{44}Sc]ScCl$_3$ at 1 h post injection. Values for each time point are given as the mean % ID per g ± 1 SD. Data for [^{44}Sc]ScCl$_3$ are taken from ref. 58.

Finally, to establish the potential use of PYTA for *in vivo* diagnostic and therapeutic applications, we performed imaging and biodistribution studies in mice with [^{44}Sc]Sc–PYTA and ^{225}Ac–PYTA, the complexes having the most extreme disparity with respect to metal-ion size. For ^{44}Sc studies, healthy female Swiss Webster mice were injected with [^{44}Sc]Sc–PYTA (~5.18 MBq) and monitored by dynamic PET imaging over the course of 55 min. Groups of mice were also sacrificed at 15 min, 1 h, and 4 h post injection, and the activity in their organs were quantified *ex vivo*. Frames across the dynamic PET acquisition (Fig. 4a) revealed uptake and localization of activity primarily in the kidneys and bladder of mice, indicative of rapid renal clearance of the intact complex. Additionally, a small amount of intestinal uptake was noted at these early time points (Fig. S38 and S39†), suggesting that some excretion also occurs through the hepatobiliary pathway. The biodistribution profile of [^{44}Sc]Sc–PYTA (Fig. 4b and Table S5†) corroborated the results of the PET imaging, showing high kidney uptake at 15 min (10.3% ID per g) that diminished over time as the complex was excreted, and a spike in intestinal activity (7.2% ID per g) at 4 h post injection. Interestingly, this gut uptake is substantially less than that observed previously for other radioscandium complexes such as [$^{43/47}$Sc]Sc–HOPO (~19% ID per g at 4 h),[57] highlighting the different pharmacokinetic properties of these complexes. Of significance, the biodistribution profile of [^{44}Sc]Sc–PYTA differs dramatically from that of free ^{44}Sc (administered as [^{44}Sc]ScCl$_3$), which exhibits a long circulation time and substantial uptake in the heart, lungs, liver, and spleen of mice (Fig. 4c).[58] Thus, the absence of accumulation of activity in these organs upon administering [^{44}Sc]Sc–PYTA to mice signifies that PYTA is able to retain ^{44}Sc *in vivo* over the time course of the study. Similar biodistribution results were obtained upon administering ^{225}Ac–PYTA (~3.7 kBq) to mice (Fig. 5 and Table S6†). Specifically, the complex was rapidly cleared through the renal system, and no activity was observed to accumulate in any organ over 48 h. This distribution pattern contrasts with that of free ^{225}Ac^{3+}, which is taken up by the liver, spleen, and bone of

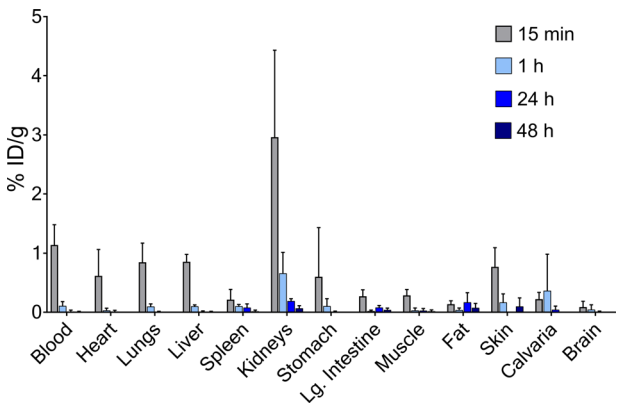

Fig. 5 *Ex vivo* biodistribution of ^{225}Ac–PYTA for select organs following intravenous injection in mice. Female Swiss Webster mice (6–8 weeks) were sacrificed 15 min, 1 h, 24 h, or 48 h post injection. Values for each time point are given as the mean % ID per g ± 1 SD ($n =$ 4).

mice.[53] The predominant renal clearance of [^{44}Sc]Sc–PYTA and ^{225}Ac–PYTA observed here in mice is similar to the biodistribution of [^{153}Sm]Sm–PYTA observed previously in rats.[30] Collectively, the results of these *in vivo* studies establish proof of concept for PYTA as a robust chelator for a complementary set of medically important radionuclides.

Conclusions

In summary, we have reported a thorough investigation of the potential of PYTA for the chelation of ^{225}Ac, ^{177}Lu, ^{111}In, and ^{44}Sc, 4 radionuclides that are of rising importance in nuclear medicine for targeted α therapy, targeted β therapy, SPECT imaging, and PET imaging, respectively. Through a dramatic change in conformation revealed by NMR and X-ray studies, PYTA can optimally accommodate and form distinct complexes with La^{3+} (as a surrogate for Ac^{3+}), Lu^{3+}, In^{3+}, and Sc^{3+}. Our studies further showed that PYTA rapidly binds this set of radiometals under mild conditions, forming complexes that are stable *in vitro* and *in vivo*. Notably, these combined results were superior to those obtained with 2 current state-of-the art chelators, DOTA and macropa, revealing PYTA as a highly versatile and effective chelator for radiotheranostic development. Future efforts are focused on preparing a bifunctional derivative of PYTA for use with tumor-targeting biomolecules.

Author contributions

The manuscript was written through contributions of all authors. All authors have given approval to the final version of the manuscript.

Conflicts of interest

There are no conflicts to declare.

Acknowledgements

Research reported in this publication was supported in part by the Laboratory Directed Research and Development Program of Oak Ridge National Laboratory (ORNL; M. E. S., M. M. S., A. S. I., F. D. W., C. M. L., N. A. T.). Additionally, A. F., Z. L., and D. L. J. T. thank the National Cancer Institute at the National Institutes of Health for support under award numbers R01CA240711 and R01CA229893. C. M. L. was supported in part by an appointment to the Oak Ridge National Laboratory GEM Fellow internship program, sponsored by the U.S. Department of Energy (DOE) and administered by the Oak Ridge Institute for Science and Education. The ^{225}Ac, ^{177}Lu, and ^{44}Ti/^{44}Sc used in this research was supplied by the DOE Isotope Program, managed by the Office of Isotope R&D and Production. This research also used resources of the Oak Ridge Leadership Computing Facility at ORNL. This work has been authored by UT-Battelle, LLC, under contract DE-AC05-00OR22725 with the U.S. DOE. The U.S. Government retains and the publisher, by accepting the article for publication, acknowledges that the U.S. Government retains a non-exclusive, paid-up, irrevocable, worldwide license to publish or reproduce the published form of this manuscript, or allow others to do so, for U.S. Government purposes. The DOE will provide public access to these results of federally sponsored research in accordance with the DOE Public Access Plan (**https://energy.gov/downloads/doe-public-access-plan**).

References

1 P. J. Blower, *Dalton Trans.*, 2015, **44**, 4819–4844.
2 T. I. Kostelnik and C. Orvig, *Chem. Rev.*, 2019, **119**, 902–956.
3 N. Herrero Álvarez, D. Bauer, J. Hernández-Gil and J. S. Lewis, *ChemMedChem*, 2021, **16**, 2909–2941.
4 M. Radzina, L. Saule, E. Mamis, U. Koester, T. E. Cocolios, E. Pajuste, M. Kalnina, K. Palskis, Z. Sawitzki, Z. Talip, M. Jensen, C. Duchemin, K. Leufgen and T. Stora, *EJNMMI Radiopharm. Chem.*, 2023, **8**, 27.
5 S. L. Pimlott and A. Sutherland, *Chem. Soc. Rev.*, 2011, **40**, 149–162.
6 J.-P. Pouget and J. Constanzo, *Front. Med.*, 2021, **8**, 692436.
7 B. M. Bavelaar, B. Q. Lee, M. R. Gill, N. Falzone and K. A. Vallis, *Front. Pharmacol.*, 2018, **9**, 996.
8 F. Roesch and M. Martin, *J. Radioanal. Nucl. Chem.*, 2023, **332**, 1557–1576.
9 L. Bodei, K. Herrmann, H. Schöder, A. M. Scott and J. S. Lewis, *Nat. Rev. Clin. Oncol.*, 2022, **19**, 534–550.
10 E. W. Price and C. Orvig, *Chem. Soc. Rev.*, 2014, **43**, 260–290.
11 E. Boros and J. P. Holland, *J. Label. Compd. Radiopharm.*, 2018, **61**, 652–671.
12 I. Carbo-Bague and C. F. Ramogida, in *Encyclopedia of Inorganic and Bioinorganic Chemistry*, ed. R. A. Scott, John Wiley & Sons, Ltd, 2021, pp. 1–34.
13 A. Hu and J. J. Wilson, *Acc. Chem. Res.*, 2022, **55**, 904–915.
14 A. Hu, S. N. MacMillan and J. J. Wilson, *J. Am. Chem. Soc.*, 2020, **142**, 13500–13506.
15 A. Hu, E. Aluicio-Sarduy, V. Brown, S. N. MacMillan, K. V. Becker, T. E. Barnhart, V. Radchenko, C. F. Ramogida, J. W. Engle and J. J. Wilson, *J. Am. Chem. Soc.*, 2021, **143**, 10429–10440.
16 A. Hu, M. E. Simms, V. Kertesz, J. J. Wilson and N. A. Thiele, *Inorg. Chem.*, 2022, **61**, 12847–12855.
17 R. D. Shannon, *Acta Crystallogr., Sect. A: Cryst. Phys., Diffr., Theor. Gen. Crystallogr.*, 1976, **32**, 751–767.
18 P. Cieslik, M. Kubeil, K. Zarschler, M. Ullrich, F. Brandt, K. Anger, H. Wadepohl, K. Kopka, M. Bachmann, J. Pietzsch, H. Stephan and P. Comba, *J. Am. Chem. Soc.*, 2022, **144**, 21555–21567.
19 I. Kopp, P. Cieslik, K. Anger, T. Josephy, L. Neupert, G. Velmurugan, M. Gast, H. Wadepohl, S. A. Brühlmann, M. Walther, K. Kopka, M. Bachmann, H. Stephan, M. Kubeil and P. Comba, *Inorg. Chem.*, 2023, **62**, 20754–20768.
20 L. Wharton, M. d. G. Jaraquemada-Pelaéz, C. Zhang, J. Zeisler, C. Rodríguez-Rodríguez, M. Osooly, V. Radchenko, H. Yang, K.-S. Lin, F. Bénard, P. Schaffer and C. Orvig, *Bioconjugate Chem.*, 2022, **33**, 1900–1921.

21 L. Wharton, H. Yang, M. d. G. Jaraquemada-Pelaéz, H. Merkens, G. Engudar, A. Ingham, H. Koniar, V. Radchenko, P. Kunz, P. Schaffer, F. Bénard and C. Orvig, *J. Med. Chem.*, 2023, **66**, 13705–13730.
22 U. Hennrich and K. Kopka, *Pharmaceuticals*, 2019, **12**, 114.
23 U. Hennrich and M. Benešová, *Pharmaceuticals*, 2020, **13**, 38.
24 U. Hennrich and M. Eder, *Pharmaceuticals*, 2022, **15**, 1292.
25 Society of Nuclear Medicine and Molecular Imaging, *J. Nucl. Med.*, 2022, **63**(5), 13N.
26 C. B. Johnbeck, U. Knigge, A. Loft, A. K. Berthelsen, J. Mortensen, P. Oturai, S. W. Langer, D. R. Elema and A. Kjaer, *J. Nucl. Med.*, 2017, **58**, 451–457.
27 O. O. Krasnovskaya, D. Abramchuck, A. Erofeev, P. Gorelkin, A. Kuznetsov, A. Shemukhin and E. K. Beloglazkina, *Int. J. Mol. Sci.*, 2023, **24**, 9154.
28 B. J. B. Nelson, J. D. Andersson and F. Wuest, *Pharmaceutics*, 2021, **13**, 49.
29 A. Jang, A. T. Kendi, G. B. Johnson, T. R. Halfdanarson and O. Sartor, *Int. J. Mol. Sci.*, 2023, **24**, 11626.
30 W. D. Kim, G. E. Kiefer, F. Maton, K. McMillan, R. N. Muller and A. D. Sherry, *Inorg. Chem.*, 1995, **34**, 2233–2243.
31 L. Miao, D. Bell, G. L. Rothremel Jr, L. H. Bryant Jr, P. M. Fitzsimmons and S. C. Jackels, *Supramol. Chem.*, 1996, **6**, 365–373.
32 L. Valencia, J. Martinez, A. Macías, R. Bastida, R. A. Carvalho and C. F. G. C. Geraldes, *Inorg. Chem.*, 2002, **41**, 5300–5312.
33 R. Bastida, D. E. Fenton, M. López-Deber, A. Macías, L. Valencia and M. Vicente, *Inorg. Chim. Acta*, 2003, **355**, 292–301.
34 M. D. C. Fernández-Fernández, R. Bastida, A. Macías, P. Pérez-Lourido, C. Platas-Iglesias and L. Valencia, *Inorg. Chem.*, 2006, **45**, 4484–4496.
35 C. Núñez, R. Bastida, A. Macías, M. Mato-Iglesias, C. Platas-Iglesias and L. Valencia, *Dalton Trans.*, 2008, 3841–3850.
36 G. Castro, M. Regueiro-Figueroa, D. Esteban-Gõmez, R. Bastida, A. Macías, P. Pérez-Lourido, C. Platas-Iglesias and L. Valencia, *Chem.–Eur. J.*, 2015, **21**, 18662–18670.
37 G. Castro, M. Regueiro-Figueroa, D. Esteban-Gómez, P. Pérez-Lourido, C. Platas-Iglesias and L. Valencia, *Inorg. Chem.*, 2016, **55**, 3490–3497.
38 G. Castro, G. Wang, T. Gambino, D. Esteban-Gómez, L. Valencia, G. Angelovski, C. Platas-Iglesias and P. Pérez-Lourido, *Inorg. Chem.*, 2021, **60**, 1902–1914.
39 C. Harriswangler, L. Caneda-Martínez, O. Rousseaux, D. Esteban-Gómez, O. Fougère, R. Pujales-Paradela, L. Valencia, M. I. Fernández, N. Lepareur and C. Platas-Iglesias, *Inorg. Chem.*, 2022, **61**, 6209–6222.
40 G. L. Rothermel Jr, L. Miao, A. L. Hill and S. C. Jackels, *Inorg. Chem.*, 1992, **31**, 4854–4859.
41 B. W. Stein, A. Morgenstern, E. R. Batista, E. R. Birnbaum, S. E. Bone, S. K. Cary, M. G. Ferrier, K. D. John, J. L. Pacheco, S. A. Kozimor, V. Mocko, B. L. Scott and P. Yang, *J. Am. Chem. Soc.*, 2019, **141**, 19404–19414.
42 G. J.-P. Deblonde, M. Zavarin and A. B. Kersting, *Coord. Chem. Rev.*, 2021, **446**, 214130.
43 R. G. Pearson, *J. Am. Chem. Soc.*, 1963, **85**, 3533–3539.
44 R. G. Parr and R. G. Pearson, *J. Am. Chem. Soc.*, 1983, **105**, 7512–7516.
45 R. G. Pearson, *Inorg. Chem.*, 1988, **27**, 734–740.
46 R. S. Drago, G. C. Vogel and T. E. Needham, *J. Am. Chem. Soc.*, 1971, **93**, 6014–6026.
47 R. D. Hancock and F. Marsicano, *Inorg. Chem.*, 1978, **17**, 560–564.
48 R. D. Hancock and F. Marsicano, *Inorg. Chem.*, 1980, **19**, 2709–2714.
49 A. E. Martell and R. D. Hancock, *Metal Complexes in Aqueous Solutions*, Plenum Press, New York, 1996.
50 H. R. Maecke, A. Riesen and W. Ritter, *J. Nucl. Med.*, 1989, **30**, 1235–1239.
51 T. J. Wadas, E. H. Wong, G. R. Weisman and C. J. Anderson, *Chem. Rev.*, 2010, **110**, 2858–2902.
52 L. Branco, J. Costa, R. Delgado, M. G. B. Drew, V. Félix and B. J. Goodfellow, *J. Chem. Soc., Dalton Trans.*, 2002, 3539–3550.
53 N. A. Thiele, V. Brown, J. M. Kelly, A. Amor-Coarasa, U. Jermilova, S. N. MacMillan, A. Nikolopoulou, S. Ponnala, C. F. Ramogida, A. K. H. Robertson, C. Rodríguez-Rodríguez, P. Schaffer, C. Williams Jr, J. W. Babich, V. Radchenko and J. J. Wilson, *Angew. Chem., Int. Ed.*, 2017, **56**, 14712–14717.
54 E. Aluicio-Sarduy, N. A. Thiele, K. E. Martin, B. A. Vaughn, J. Devaraj, A. P. Olson, T. E. Barnhart, J. J. Wilson, E. Boros and J. W. Engle, *Chem.–Eur. J.*, 2020, **26**, 1238–1242.
55 F. Reissig, D. Bauer, M. Ullrich, M. Kreller, J. Pietzsch, C. Mamat, K. Kopka, H.-J. Pietzsch and M. Walther, *Pharmaceuticals*, 2020, **13**, 272.
56 D. S. Abou, N. A. Thiele, N. T. Gutsche, A. Villmer, H. Zhang, J. J. Woods, K. E. Baidoo, F. E. Escorcia, J. J. Wilson and D. L. J. Thorek, *Chem. Sci.*, 2021, **12**, 3733–3742.
57 M. D. Phipps, S. Cingoranelli, N. V. S. D. K. Bhupathiraju, A. Younes, M. Cao, V. A. Sanders, M. C. Neary, M. H. Devany, C. S. Cutler, G. E. Lopez, S. Saini, C. C. Parker, S. R. Fernandez, J. S. Lewis, S. E. Lapi, L. C. Francesconi and M. A. Deri, *Inorg. Chem.*, 2023, **62**, 20567–20581.
58 N. Benabdallah, H. Zhang, R. Unnerstall, A. Fears, L. Summer, M. Fassbender, B. E. Rodgers, D. Abou, V. Radchenko and D. L. J. Thorek, *EJNMMI Res.*, 2023, **13**, 17.